Excellent Photostability of Phosphorescent Nanoparticles and Their Application as a Color Converter in Light Emitting Diodes

Ok-Hee Kim, Shin-Woo Ha,[†] Jae Il Kim, [‡] and Jin-Kyu Lee*

Department of Chemistry, Seoul National University, Seoul 151-747, Korea. [†]Current address: Department of Materials Science and Engineering, Seoul National University, Seoul 151-744, South Korea. [‡]Current address: Analytic Research Group, Corporate R&D Institute, Samsung Electro-Mechanics Co., Ltd., Suwon 443-743, South Korea.

A mong the many phosphorescent metal complexes, Ir(III) complexes have several advantages such as intense phosphorescence with a high quantum yield at room temperature, luminescent colors that can be tuned by modifying ligand systems, and a relatively long phosphorescent lifetime due to the close proximity of the ligand-centered (^{3}LC) and metal-to-ligand charge transfer (^{3}MLCT) excited states and the large spin−orbit coupling constant of Ir^{3+}, which induce a strong mixing of the charge-transfer character into the lowest ^{3}LC excited states.[1−4] Owing to these advantages, Ir(III) complexes have been investigated as attractive phosphorescent materials for various applications such as organic light-emitting devices (OLED),[5−10] light-emitting electrochemical cells (LEC),[11,12] electrogenerated chemiluminescence (ECL),[13−15] and biological staining and monitoring systems.[16−20] Although they possess superior photophysical properties such as long lifetime, notably large Stokes shift, high stability, and lower self-quenching as compared to conventional organic fluorophores,[21] Ir(III) complexes have some drawbacks for biological applications since they are poorly soluble in aqueous solutions and are easily quenched by the oxygen in air, owing to their long lifetime in the triplet state. By incorporating the Ir(III) complexes into a silica matrix to isolate them from oxygen and other external quenchers, the quenching process of the Ir(III) complexes could be effectively restrained and their photophysical, thermal, and optical stability could be significantly enhanced as compared to those of the com-
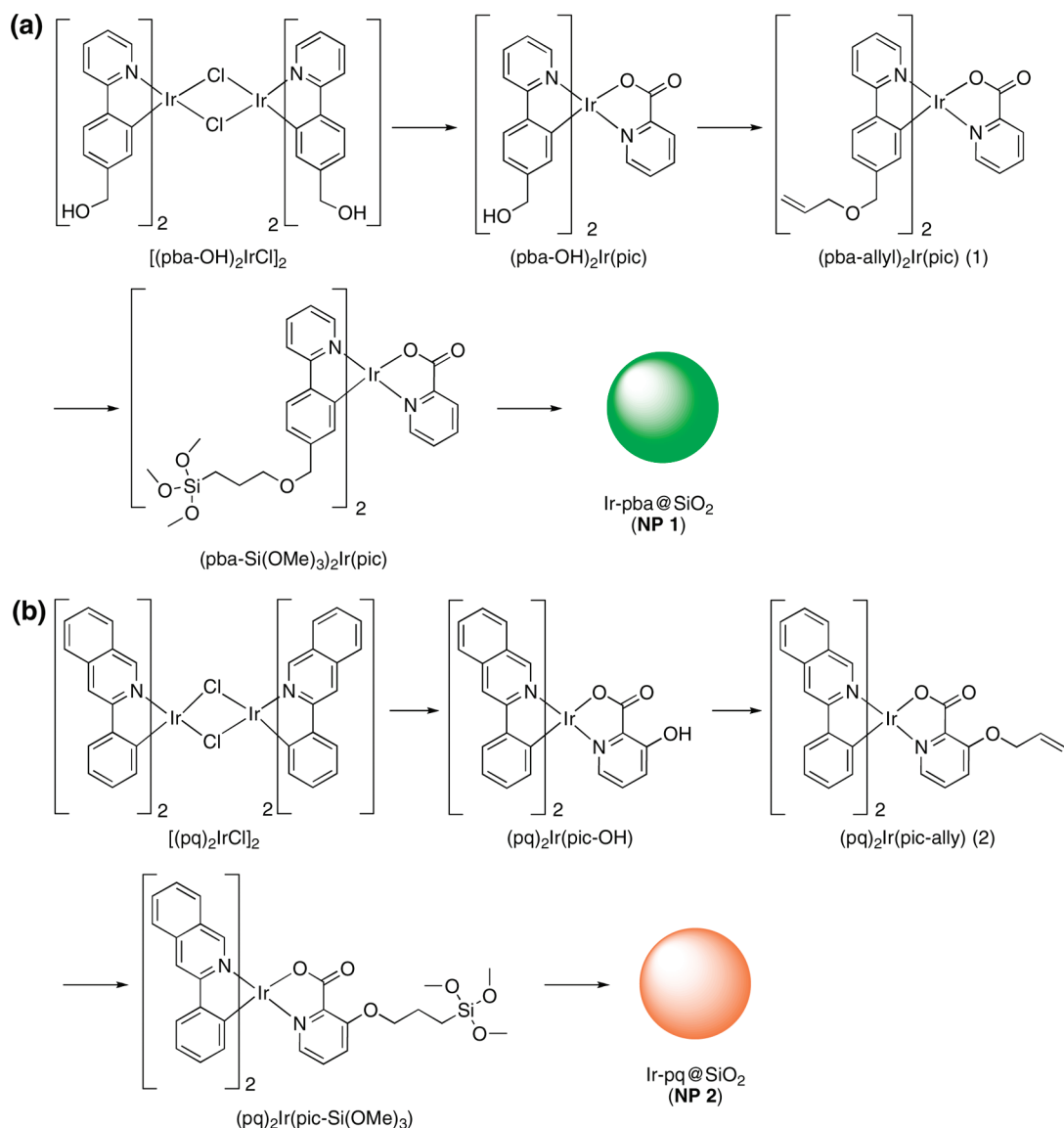
plexes in solution states.[22−24] Moreover, the use of silica shell as a matrix provides several other benefits: enhanced dispersibility in water, biocompatibility, chemical and mechanical stability, and the possibility of further functionalization through the modification of the silica surface.[25] Since the lack of covalent bonding between dyes and matrices imposes a limitation on the amount of dye molecules that can be incorporated and since the physisorbed dye molecules tend to leak out of the particles over time, the induction of covalent bonding between the incorporated dye molecules and the silica matrix by coupling the derivatized dyes with reactive organosilicon reagents to form a thiourea linkage has been suggested.[26,27] Although the thiourea-linkage formation reaction, which employs an amino-terminated alkyltrialkoxysilane compound such as aminopropyltriethoxysilane (APS) and dye molecules that have an isothiocyanate functional group, is simple

ABSTRACT The phosphorescent Ir(III) complexes were modified by allylation and consecutive hydrosilylation, and covalently incorporated into the silica nanoparticles by hydrolysis and condensation reaction with TEOS. These nanoparticles showed an excellent photochemical and thermal stability, and a very high luminescent efficiency due to the blocking of O$_2$ quenching and suppression of energy transfer through the amorphous silica solid solution. The limited mobility of complexes in the silica matrix also resulted in a decrease in the vibration relaxation and restrained the nonradiative decay. It is expected that these photostable and very efficient phosphorescent nanoparticles can be used in various fields ranging from nanobiotechnology to nanoengineering materials, where long-term stability with the high luminescent efficiency is required. As an example of the use of excellent photostability, a preliminary test result in which they are used as a color converter in a light emitting diode (LED) is also discussed.

KEYWORDS: phosphorescent nanoparticles · iridium(III) complex · silica nanoparticles · luminescence · photostability · LED color converter

Scheme 1. Synthetic routes of green (a) and red (b) phosphorescent silica nanoparticles containing Ir(III) complexes.

and has been well studied as a useful conjugation method in many applications, it has several drawbacks in the preparation of stable fluorescent silica nanoparticles. Therefore, the method of direct derivatization of dye molecules by consecutive allylation and hydrosilylation has been developed recently to prepare fluorescent silica nanoparticles with excellent photostability and biocompatibility.[28]

In this paper, we report a novel synthetic method for the preparation of phosphorescent silica nanoparticles having Ir(III) complexes by the direct derivatization of ligands, and their photostability of phosphorescent silica nanoparticles which is required for multiple-time monitoring in order to investigate the differentiation and/or development of cells. As an example of the use of excellent photostability of prepared phosphorescent nanoparticles, a preliminary test result in which they are used as a color converter in a light emitting diode (LED) is also discussed.

RESULTS AND DISCUSSION

The synthesis of green-emitting Ir(III) complex (pba-allyl)$_2$Ir(pic) (**1**; Hpba = 4-(2- pyridyl)benzaldehyde; pic = picolinic acid; Scheme 1) was started from a dimeric form of [(pba)$_2$IrCl]$_2$ since it has two reactive aldehyde groups that can be conveniently converted to a hydroxyl group by reduction with NaBH$_4$. After a monomeric complex was formed using 2-picolinic acid as an ancillary ligand, the allylation of hydroxyl groups in the main ligands was achieved by refluxing with a strong base of tertiary butoxide in a THF solvent and reacting it with allyl iodide. The other allyl-functionalized red-emitting Ir(III) complex, (pq)$_2$Ir(pic-allyl) (**2**; Hpq = 2-phenylquinoline) was prepared from [(pq)$_2$IrCl]$_2$. 3-Hydroxypicolinic acid was used as an ancillary ligand because its hydroxyl group could be easily deprotonated with Cs$_2$CO$_3$ in DMF and reacted with allyl iodide. This method in which 3-hydroxypicolinic acid is used as an ancillary ligand for the allylation could be ex-
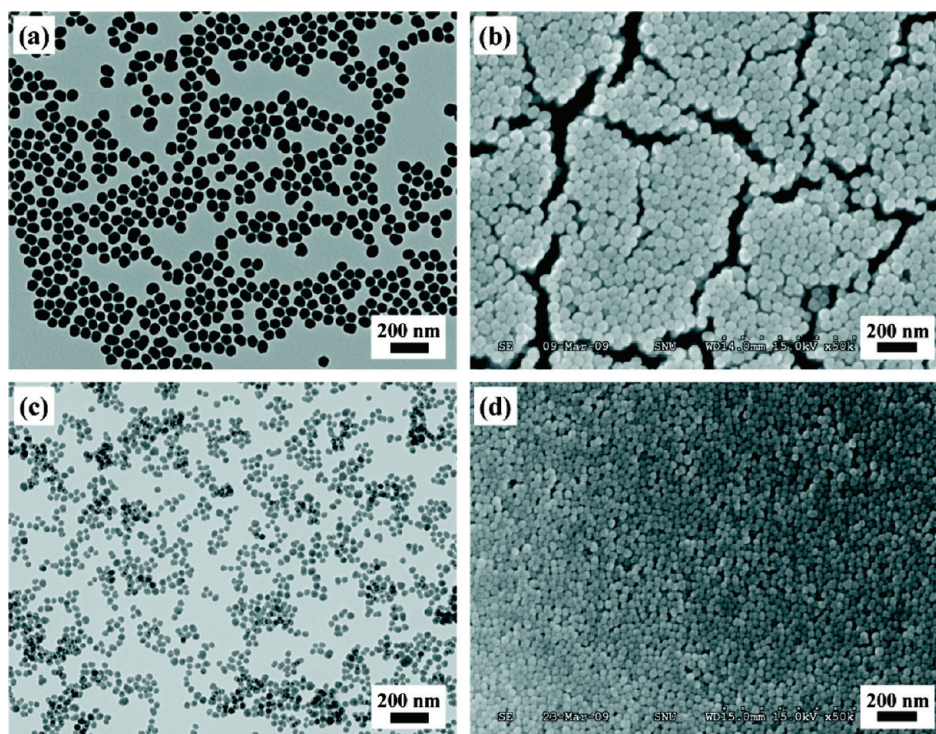
Figure 1. TEM and FE-SEM images of phosphorescent silica nanoparticles: TEM images of (a) NP1 and (c) NP2, and FE-SEM images of (b) NP1 and (d) NP2.

tended to most Ir(III) complexes, which promises the possibility of various color-tuning applications. Complexes **1** and **2**, including the intermediates, were characterized by ^{1}H NMR and FAB-MS or MALDI-TOF. From the allylated complexes, the hydrosilylation reaction was performed with trimethoxylsilane in the presence of a platinum catalyst. Phosphorescent silica nanoparticles were successfully prepared by the modified Stöber method,[29] which involves the hydrolysis and condensation of tetraethyl orthosilicate (TEOS) and directly derivatized Ir(III) complexes in ethanol with NH₄OH and water. The prepared nanoparticles were isolated and purified by centrifugation and subsequent wash-

ing with ethanol several times. The size and the size distribution of **NP1** and **NP2** were characterized by transmission electron microscopy (TEM) and field-emission scanning electron microscopy (FE-SEM). Both nanoparticles were monodisperse and spherical, and their size was 52 ± 6 and 40 ± 10 nm, respectively, in diameter (Figure 1). The size of the silica nanoparticles could be controlled in a range of 20 nm to a few hundred nanometers by varying the concentrations of TEOS, water, and ammonia as reported in the literature.[28]

The photoluminescence spectra of **1**, **2**, **NP1**, and **NP2** are shown in Figure 2, and the photophysical data are listed in Table 1. Complexes **1** and **2** showed green
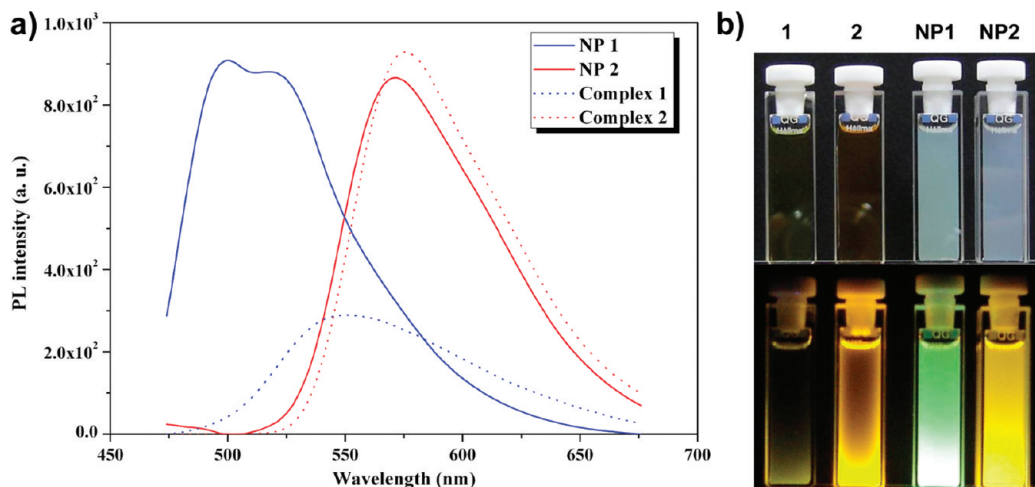

Figure 2. (a) Emission spectra of complexes 1 and 2 in CHCl₃ and NP1 and NP2 in ethanol at room temperature. (b) Photographs of the complexes (1 and 2) and the nanoparticles (NP1 and NP2) under natural light (above) and under UV irradiation at 365 nm (below).

TABLE 1. Photophysical Properties of Ir(III) Complexes (1 and 2) and Nanoparticles (NP1 and NP2)

name	$\lambda_{PL,\ max}$ (nm)	rel $\Phi_{PL}{}^a$	τ_1 $(\mu s)^b$	τ_2 $(\mu s)^b$
Complex **1**	559	0.002	1.32	10.3
NP1	501	0.040	2.97	10.0
Complex **2**	576	0.056	1.48	10.6
NP2	571	0.075	2.50	10.0

^{a}Values were obtained in ethanol using an inorganic complex, comparing to [Ru(bpy)$_3$]Cl$_2$ in water (Φ_{PL} = 0.028) as a standard.[30] ^{b}Lifetimes were obtained by biexponential fit of emission curve. All samples were measured in air-saturated solvent: ethanol in all the quantum yield measurements, ethanol for complex 1 and 2 and CHCl$_3$ for NP1 and NP2 in life-time measurements.

(λ_{max} = 548 nm, in CHCl$_3$) and red (λ_{max} = 574 nm, in CHCl$_3$) emissions in the PL spectra, respectively. The maximum emission wavelength of **NP1** was observed at ~500 nm, shifting to a higher energy than that of complex **1**, while the intensity of photoluminescence intensity and the quantum efficiency of **NP1** was about 3 times higher than those of complex **1**. This could be explained by the fact that the encapsulated complex **1** in the silica matrix had restricted contact with the oxygen quencher in the system. Furthermore, the limited mobility of complex **1** in the silica matrix resulted in a decrease in the vibration relaxation and restrained the
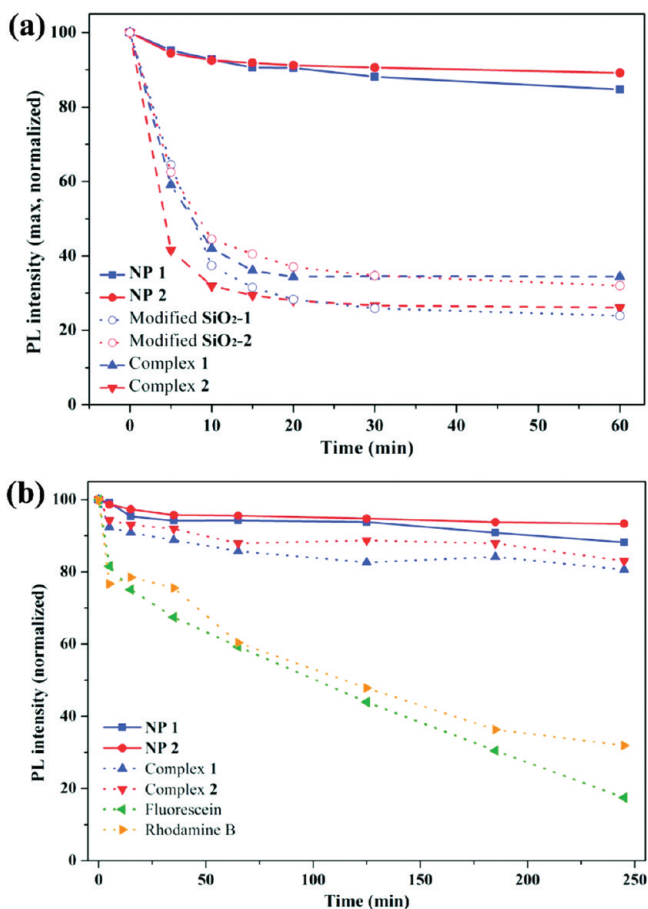

Figure 3. (a) Decay plot of PL intensity in ethanol at room temperature; all solutions were degassed by N$_2$ bubbling and then left in contact with O$_2$ in air. (b) Photobleaching experiment by W-halogen lamp (200 W, KANDO lite) at an intensity of 757 mW/cm^2

nonradiative decay. The pseudosolid state environment ensured a separation between neighboring Ir(III) complexes and also suppressed energy transfer and quenching, as reported in the literature.[22–24] In the case of complex **2** and **NP2**, on the other hand, no significant enhancement was observed, probably because complex **2** already had high phosphorescence quantum efficiency due to its rigid structure with bulky ligands. A very slight shift to a higher energy in the PL spectra also suggests that the restriction of mobility in complex **2** did not appreciably change after its incorporation in the solid silica matrix. The excited state lifetimes of all samples were measured on the time scale of microseconds, which is the major characteristic of phosphorescent materials (Table 1). Although the differences in lifetime among complexes **1**, **2**, **NP1**, and **NP2** were not significant, the τ_1 values of **NP1** and **NP2** were about twice as large as those of complexes **1** and **2**. It is expected that τ_1 values are related with O$_2$ quenching, thereby supporting the effect of confinement by the surrounding nonporous silica matrix.

To quantitatively measure the enhancement of the PL of **NP1** and **NP2**, quenching experiments with oxygen were performed. After each solution of the complexes and nanoparticles was bubbled with N$_2$ for 30 min to remove most of the dissolved oxygen, the PL intensities of each solution reached their maximum value. By removing the caps, the solutions of each sample were allowed to make contact with oxygen in air, and their PL intensity was measured over time (Figure 3a). The PL intensities of complexes **1** and **2** decreased rapidly within 10 min to about 40 and 30%, respectively, of their original intensities, and reached their equilibrium values of 34 and 26%, respectively, after 20 min. The PL intensities of nanoparticles **NP1** and **NP2**, on the other hand, slightly decreased to about 90% of their starting maximum values after 20 min, and finally reached their equilibrium values of 85 and 89%, respectively, after 60 min. This enhanced phosphorescence efficiency for **NP1** and **NP2** could have resulted from the effect of confinement by the surrounding solid silica matrix, which isolated complexes **1** and **2** from the oxygen quencher molecules. The surfaces of similarly sized pure silica nanoparticles (~50 nm) were modified with Ir(III) complexes **1** and **2** in order to compare the photoluminescence quenching of the Ir(III) complexes when they are attached to the surface or near the surface, as pointed out in the literature.[24] Surface modified nanoparticles were prepared by refluxing hydrosilylated Ir(III) complexes and pure silica nanoparticles in ethanol for 2 days (modified **SiO$_2$-1** and modified **SiO$_2$-2**). Since Ir(III) complexes existed only on the surface of the silica nanoparticle, they were not protected by the silica matrix and no enhancement of photoluminescence was observed; the PL intensity of modified **SiO$_2$-1** and modified **SiO$_2$-2** decreased to 23 and 31%, respectively, of their original values within 20 min, which is very simi-

lar to the values for complexes **1** and **2** themselves (Figure 3a). In the case of **NP1** and **NP2**, it could be explained that the slight reduction in PL intensity (11 or 15%, respectively) might result from the Ir(III) complexes located on the surface, and that most of the complexes were incorporated inside the silica matrix.

The excellent photostability of **NP1** and **NP2** was confirmed by photobleaching experiments. All the sample solutions were exposed to UV light from a W-halogen lamp, and the PL intensities were measured over time in order to compare their photodegradation (photobleaching) kinetics. Even though the Ir(III) complexes have very good photostability, as has been reported,[31] compared to well-known organic fluorescent molecules such as rhodamine B and fluorecein, as shown in Figure 3b, **NP1** and **NP2** wherein the Ir(III) complexes are embedded in the SiO_2 matrix show even better photostability after continuous irradiation by UV light for 4 h. The normalized PL intensities of **NP1** and **NP2** maintained an almost constant value of 88 and 97% of their starting intensities, respectively, after 4 h of continuous irradiation, while those of Ir(III) complexes **1** and **2** decreased to ~83% and those of rhodamine B and fluorecein molecules dropped to 10−30% of their original intensities. These results for the dye molecules were consistent with those in previous reports.[28,32] In addition to the enhancement of PL intensity and excellent photostability, **NP1** and **NP2** also exhibited good thermal stability. When **NP1** was heated in a furnace at 120 °C for 18 h and then further heated at 200 °C for 1 h, only slight changes in phosphorescent intensity were observed, even though some nanoparticles were aggregated during the heat treatment. At a high temperature of over 300 °C, however, the PL intensity began to decrease with time (Figure 4a).

For a quantitative analysis of the amount of Ir(III) complexes incorporated in the silica matrix, a calibration curve was prepared for PL intensity *versus* concentration for complexes **1** and **2**. It was assumed that the absorption and emission coefficients were the same irrespective of whether the Ir(III) complexes were dissolved in ethanol or in a supernatant solution (mostly ethanol and some water and ammonia). By measuring the differences in PL intensity between the solution, before the start of the SiO_2 formation, and the supernatant, after the collection of the generated SiO_2, the amount of incorporated Ir(III) complexes could be calculated. The weight ratio of the complexes incorporated in silica nanoparticles was increased as the amount of the hydrosilylated Ir(III) complexes was increased in starting reaction mixtures. The weight ratio of the Ir(III) complex could be increased to 26 wt % in our experiments. When more Ir(III) complexes were used, however, the size control of the generated silica particles was affected, thereby resulting in a wider distribution.
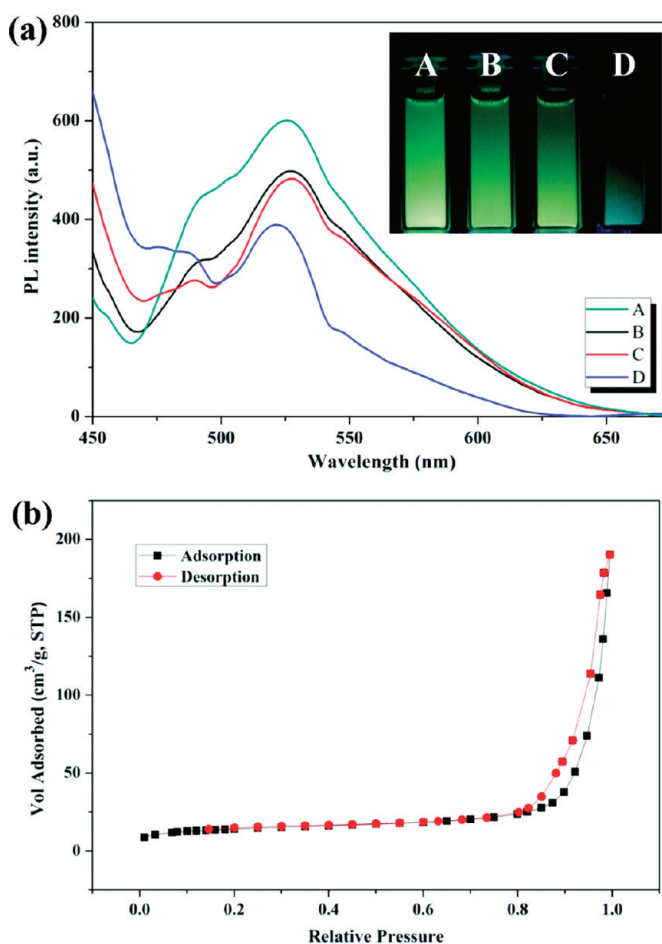

Figure 4. (a) Thermal stability of **NP1** (A, reference; B, 120 °C; C, 200 °C; D, 300 °C). The concentration was 1.68 mg/mL in ethanol. Inset: photos under UV irradiation at 365 nm. (b) Plot of physisorption isotherms of N_2 at 77 K on **NP1**.

On the basis of the stable phosphorescence of **NP1** and **NP2** in the quenching experiments, we postulated that the incorporated Ir(III) complexes are effectively protected from contact with oxygen and other quenchers because silica nanoparticles prepared by the Stöber method are usually assumed to have nonporous amorphous form. To confirm the porosity of the prepared silica nanoparticles, the surface area was measured by nitrogen adsorption isotherms and the BET equation. The BET surface area of **NP1** was measured as 49.6 m^2/g and the Langmuir surface area was calculated as 67.8 m^2/g; it was thus determined that the type of physisorption isotherms of **NP1** was type-II, which is a normal form of isotherm for a nonporous or macroporous adsorbent (Figure 4b).[33] It was then concluded that **NP1** must be nonporous in order to protect the Ir(III) complexes with suitable environment from external perturbations.

Since phosphorescent Ir(III) complexes that are prepared by direct modification and that are chemically embedded in the solid silica matrix possess excellent photostability and present no photobleaching problems, the phosphorescent silica nanoparticles **NP1** and
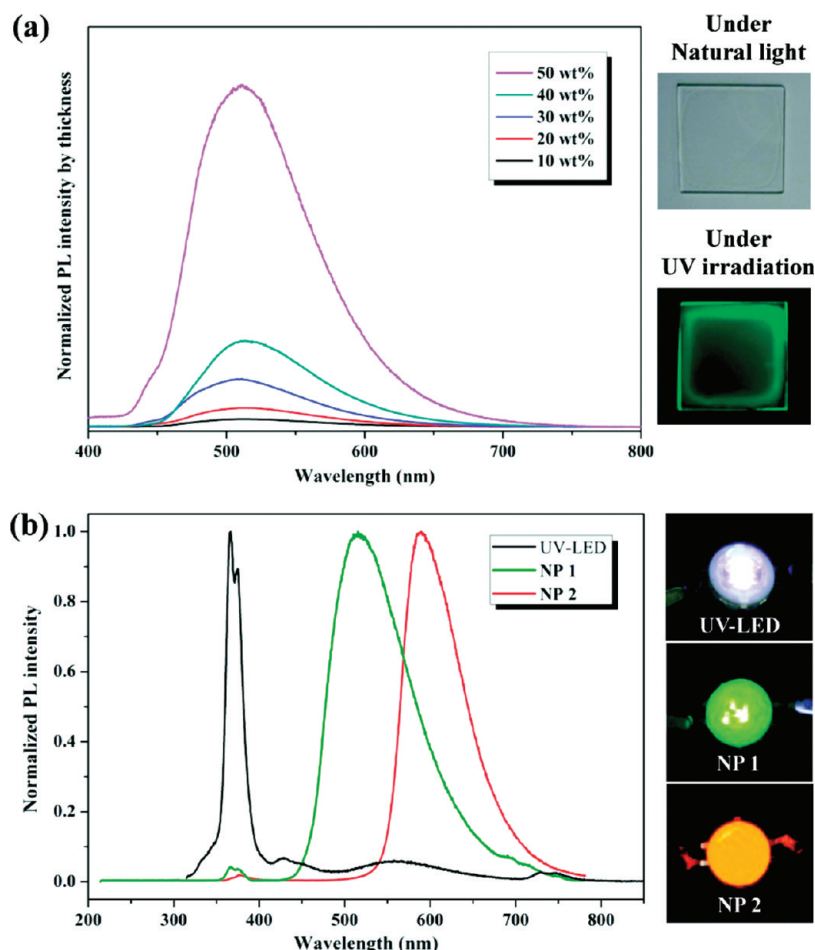
Figure 5. (a) Emission spectra of **NP1**—polymer nanocomposite thin films depending on the **NP1** contents. Inset: photos of **NP1**—polymer nanocomposite films on quartz under natural light (above) and UV irradiation (below). (b) Emission spectra of **NP1**—polymer and **NP2**—polymer nanocomposites on UV-LED devices. Inset: photos of **NP1**—polymer (middle) and **NP2**—polymer (below) nanocomposites on the devices.

NP2 are expected to be biocompatible, as has been reported.[28] They could therefore be used as efficient luminescent tagging reagents for biological experiments in which multiple-time monitoring to investigate the differentiation and/or development of cells is required.

With such great photostability and high phosphorescent efficiency, an interesting application of **NP1** and **NP2** could be as a color converter material in LED display devices. We conducted a preliminary test that was designed to explore this possibility. First, the phosphorescent silica nanoparticles were mixed with a polyvinyl alcohol (PVA, average $M_w = 13k$) binder to fabricate nanocomposite thin films. **NP1**—PVA nanocomposite thin films with various levels of **NP1** content were fabricated on quartz substrates by the spin-coating method, and their PL spectra were measured. As the **NP1** content was increased, the actual thickness of the spin-coated thin film increased to a maximum value of around a few micrometers in the case of 30 wt % composite film. However, the thickness tended to decrease as the **NP1** content was further increased, probably due to the low viscosity of the composite solution as the relative amount of PVA progressively decreased. The actual thickness of the 50 wt

% composite film was around 80 nm, which corresponds to mono- or bilayers of nanoparticles. It was clearly observed that the PL intensities increased as a function of the wt% of **NP1** (Figure 5a) when the intensities were normalized with the film thickness. As expected, by increasing the **NP1** content while decreasing the film thickness, a more closely packed arrangement of **NP1** could be achieved to give a higher phosphorescent intensity per unit thickness of the film. This would be critical to the fabrication of color converter layers onto the top of UV-LEDs; when nanoparticles are used, because of their small size, the absorption cross section of the composite film tends to be small and the color conversion efficiency is not sufficiently high.

Composite films with 50 wt % of **NP1** and **NP2** were coated onto the UV-LEDs, and the complete shift of their emission wavelengths from UV to a green and orange color, respectively, was observed (Figure 5b). The color-converted LEDs exhibited an appropriately bright and intense emission, which corresponded to the emission spectra of **NP1** and **NP2** (Figure 2a). More importantly, as observed in the color-converted emission spectra, the UV emission from the original light source was absorbed almost completely by **NP1** and **NP2**. This

is critical for the color conversion from UV-LED, and the closely packed arrangement of phosphorescent silica nanoparticles in composite films can produce this excellent result. It is expected, therefore, that phosphorescent silica nanoparticles having excellent photostability could be used as an important color-converting material in full-color LED displays, since UV-LEDs with a phosphor mixture system provide an excellent color rendering index (CRI) value for white light or suitable applications.[34]

CONCLUSIONS

In summary, we have demonstrated that phosphorescent Ir(III) complexes can be directly derivatized with trialkoxysilane and successfully incorporated into silica nanoparticles. Since the Ir(III) complexes incorporated within the solid silica matrix could be effectively isolated from quencher molecules and sterically confined, a very strong phosphorescence was observed in the solution even in air, and excellent photostability and thermal stability were obtained. It is expected that these photostable and very efficient phosphorescent nanoparticles can be used in various fields ranging from nanobiotechnology (imaging, targeting, and sensing) to nanoengineering materials (LED color converter, photonics, and optoelectronics), where long-term stability with high luminescent efficiency is required.

METHODS

All solvents and reagents were commercially available and used without further purification unless otherwise noted. ^{1}H NMR spectra were recorded on Bruker Avance DPX-300 instruments and mass spectra were obtained using MALDI-TOF (matrix-assisted laser desorption ionization time-of-flight, Voyager-DETM STR Biospectrometry Workstation). High-resolution masses (HRMS) were measured by FAB (fast atom bombardment) MS using a JEOL JMS-AX505WA. The silica nanoparticles were characterized by a transmission electron microscope (TEM; Hitachi, H-7600) and a field emission scanning electron microscope (FE-SEM; Hitachi, S-4300). The size of the nanoparticles was analyzed by ImageJ program, which is freely available from NIH webpage (http://rsbweb.nih.gov/ij/). UV−visible spectra were measured on a Scinco 2100 spectrophotometer, and the photoluminescent spectra were measured by a Jasco FP-750 spectrofluorometer. [Ru(bpy)$_3$]Cl$_2$ was used as reference ($\Phi_{PL} = 0.028$ in air-saturated water).[30] The lifetimes were measured by TCSPC (time correlated single photon counting spectrometer, Edinburgh), and the surface area analyzer used was Micrometric's ASAP (accelerated surface area and porosimetry analyzer) 2010 model.

Synthesis of [C$^\wedge$N$_2$IrCl]$_2$. Cyclometalated iridium(III) μ-chloro-bridged dimers of general formula *C$^\wedge$N$_2$*Ir(μ-Cl)$_2$Ir*C$^\wedge$N$_2$* were synthesized by the method reported by Nonoyama,[35] which involves refluxing IrCl$_3 \cdot n$H$_2$O (STREM) with 2−2.5 equiv of cyclometalating ligand (*C$^\wedge$N* = 4-(2-pyridyl)benzaldehyde; pba, 2-phenylquinoline; pq) in a 3:1 mixture of 2-ethoxyethanol (Aldrich Sigma) and water. [(pba−OH)$_2$IrCl]$_2$ was prepared by reducing the [(pba)$_2$IrCl]$_2$ complex using excess sodium borohydride with anhydrous ethanol.

(pba−OH)$_2$Ir(pic). The chloro-bridged dimer [(pba−OH)$_2$IrCl]$_2$ complex (0.2 mmol), 0.5 mmol of picolinic acid (pic), and excess potassium carbonate were refluxed in 2-ethoxyethanol for 12 h. The colored precipitate was filtered off; washed with water, ethanol, ether, and hexane; and dissolved in dichloromethane. The crude product was purified by flash chromatography (silica/dichloromethane) or recrystallization to give a yellow powder after solvent evaporation and drying. (Yield 86%) ^{1}H NMR (300 MHz, DMSO-*d$_6$*, δ) = 8.47 (d, 1H), 8.19−8.06 (m, 4H), 7.93 (t, 1H), 7.91 (t, 1H), 7.77 (d, 1H), 7.73 (d, 1H), 7.64 (d, 1H), 7.59 (m, 1H), 7.52 (d, 1H), 7.34 (t, 1H), 7.18 (t, 1H), 6.86 (t, 2H), 6.24 (s, 1H), 6.06 (s, 1H), 4.88 (t, 1H), 4.81 (t, 1H), 4.25 (d, 2H), 4.13 (d, 2H). FAB-MS: calculated for C$_{30}$H$_{24}$IrN$_3$O$_4$ M$^+$ 683.1396; observed for M$^+$ 683.1398.

(pba-allyl)$_2$Ir(pic), complex 1. (pba−OH)$_2$Ir(pic) complex (0.2 mmol) was dissolved in anhydrous THF, and excess potassium *tert*-butoxide was added. After 30 min, 2 mL of allyl iodide was added, and then refluxed for 12 h under N$_2$. After cooling down at room temperature, the reaction mixture was carefully quenched by the slow addition of ice water. The solvent was removed under reduced pressure, and the residue was extracted with dichloromethane and water. The organic phase was dried over magnesium sulfate and removed under reduced pressure. The crude product was purified by recrystallization to give a yellow powder. (Yield 95%) ^{1}H NMR (300 MHz, DMSO-*d$_6$*, δ) = 8.49 (d, 1H), 8.20 (d, 2H), 8.13 (d, 2H), 7.92 (m, 2H), 7.76 (dd, 2H), 7.52 (t, 2H), 7.33 (t, 1H), 7.22 (t, 1H), 7.20 (t, 1H), 6.79 (t, 2H), 6.24 (s, 1H), 6.05 (s, 1H), 5.74 (m, 2H), 5.09 (d, 4H), 4.23 (s, 2H), 4.19 (s, 2H), 3.81 (t, 4H). FAB-MS: calculated for C$_{36}$H$_{32}$IrN$_3$O$_4$ M$^+$ 763.2022; observed for M$^+$ 763.2024.

(pq)$_2$Ir(pic−OH). The chloro-bridged dimer, [(pq)$_2$IrCl]$_2$ complex (0.2 mmol), 0.5 mmol of 3-hydroxy picolinic acid (pic−OH), and excess potassium carbonate were dissolved in 2-ethoxyethanol and refluxed for 12 h. After cooling down at room temperature, the solvent was evaporated under reduced pressure and dissolved in dichloromethane. The organic phase was washed with water and dried over magnesium sulfate, and the solvent was removed under reduced pressure. The crude product was purified by recrystallization to give a red powder. (Yield 86%) ^{1}H NMR (300 MHz, DMSO-*d$_6$*, δ) = 13.48 (s, 1H), 8.58 (d, 1H), 8.51−8.46 (m, 4H), 8.20 (d, 1H), 8.06−8.01 (m, 3H), 7.53 (d, 2H), 7.42 (m, 3H), 7.35 (t, 1H), 7.24 (t, 1H), 7.07 (t, 1H), 6.97 (t, 1H), 6.73 (t, 1H)), 6.63 (d, 2H), 6.14 (d, 1H). MALDI-TOF: calculated for C$_{36}$H$_{24}$IrN$_3$O$_4$ M$^+$ 739.1447; observed for M$^+$ 738.829.

(pq)$_2$Ir(pic-allyl), complex 2. (pq)$_2$Ir(pic−OH) complex (0.3 mmol) and Cs$_2$CO$_3$ (1.8 mmol) were dissolved in anhydrous DMF. After 30 min, 2 mL of allyl iodide was added and then refluxed for 12 h under N$_2$. After being cooled down at room temperature, the solvent was removed under reduced pressure, and the residue was extracted with dichloromethane and water and then washed with brine. The organic phase was dried over magnesium sulfate and the solvent was removed under reduced pressure; the crude product was purified by recrystallization to give a red powder. (Yield 95%) ^{1}H NMR (300 MHz, DMSO-*d$_6$*, δ) = 8.56 (d, 1H), 8.49 (d, 1H), 8.46 (m, 3H), 8.20 (d, 1H), 8.03 (t, 2H), 7.96 (d, 1H), 7.52−7.41 (m, 6H), 7.29 (d, 1H), 7.04 (t, 1H), 6.93 (t, 1H), 6.70 (t, 1H), 6.61 (d, 1H) 6.05 (d, 1H), 5.77 (m, 1H), 5.25 (d, 1H), 5.05 (d, 1H), 4.42 (d, 2H). MALDI-TOF: calculated for C$_{39}$H$_{28}$IrN$_3$O$_3$ M$^+$ 779.1760; observed for M$^+$ 778.763.

Hydrosilylation of the Allylated Ir(III) Complexes (1, 2). The hydrosilylation procedure was carried out in a similar way.[36] A total of 0.2 mmol of complex **1** (**2**) was dissolved in anhydrous methanol, and 0.5 mL of trimethoxysilane and 10 wt % platinum on activated carbon were added and refluxed overnight under N$_2$. After cooling down at room temperature, the catalyst was removed by filtration with a Celite pad in a glovebox. Excess trimethoxysilane and solvent were dried *in vacuo* with heat.

(pba-Si(OMe)$_3$)$_2$Ir(pic). (Yield 76%) ^{1}H NMR (300 MHz, DMSO-*d$_6$*, δ) = 8.55 (d, 1H), 8.53 (d, 2H), 8.25 (d, 2H), 7.97 (m, 2H), 7.84 (dd, 2H), 7.57 (t, 2H), 7.40 (t, 1H), 7.24 (t, 1H), 6.88 (t, 1H), 6.82 (t, 2H), 6.30 (s, 1H), 6.11 (s, 1H), 4.20 (dd, 4H), 3.37 (s, 18H), 3.24 (d, 4H), 1.42 (m, 4H), 0.81 (m, 4H).

(pq)$_2$Ir(pic-Si(OMe)$_3$). (Yield 99%) ^{1}H NMR (300 MHz, DMSO-*d$_6$*, δ) = 8.56 (d, 1H), 8.41 (d, 1H), 8.39 (m, 3H), 8.22 (d, 1H), 7.90 (t, 2H), 7.85 (d, 1H), 7.43−7.34 (m, 6H), 7.21 (d, 1H), 6.96 (t, 2H), 6.85 (t, 1H), 6.53 (t, 1H), 6.47 (t, 2H) 5.98 (d, 1H), 3.77 (s, 2H), 3.25 (s, 9H), 1.31 (m, 2H), 0.75 (m, 2H).

Synthesis of Phosphorescent Silica Nanoparticles. A total of 0.1 mmol of the hydrosilylated iridium(III) complexes and 2.0 mL of tetraethyl orthosilicate (TEOS) were dissolved in 118 mL of dried ethanol, and 2.5 mL of ammonia and 2.5 mL of water were added while stirring at 400 rpm. After being stirred for 1 day, the iridium(III) complexes that encapsulated the silica nanoparticles were isolated by centrifugation at 15 000 rpm and the supernatant was disposed of. The isolated products were washed with and redispersed in ethanol. The washing and redispersion were repeated for three times. Finally, the nanoparticle solution was centrifuged at 4000 rpm to remove some aggregated particles. The purified silica nanoparticles were dispersed in the desired solvents such as ethanol, water, and a buffer.

Quantification of the Encapsulated Ir(III) Complexes in Silica Nanoparticles. A total of 0.8 mL of tetraethyl orthosilicate (TEOS) and various molar ratios of hydrosilylated Ir(III) complexes were mixed in 47.2 mL of dried ethanol, 1.0 mL of ammonia, and 1.0 mL of water. We calculated the amount of the remaining Ir(III) complexes in the supernatant by using a calibration curve, thus, comparing the differences before and after the reaction. The amount of Ir(III) complexes in SiO$_2$ was also determined. The encapsulated Ir(III) complexes and the weight ratio of iridium(III) complexes and silica nanoparticles increased as the amount of Ir(III) complexes at the start was increased. The weight ratio of the Ir(III) complex could be increased to 26 wt % in our experiment; when more iridium(III) complexes were used, the size control of the generated silica particles was affected, thereby resulting in a wider distribution.

Thermal Stability Test. The solid-form **NP1** was isolated by centrifugation at 18 000 rpm for 30 min, and the supernatant was discarded. The isolated silica nanoparticles were dried in air for 1 day. A total of 8.4 mg of solid **NP1** was heated in a furnace to 120 °C for 18 h (B), and then further heated to 200 °C (C), and 300 °C for 1 h in furnace (D). They were then redispersed in 5 mL of ethanol with sonication for 5 h.

Porosity Measurement of NP1. The sample (solid-form **NP1**) was dried at 100 °C for 24 h in a furnace and at 200 °C for 3 h less than 20 mmTorr before measurement in order to clean the surface of the sample. Nitrogen was used as the analytical gas. It took about 7−12 h to complete an adsorption−desorption isotherm at 77 K. The surface area was determined on the basis of the amount of gas adsorbed at a given pressure. This value was observed to be different from that calculated by the BET (Brunauer−Emmett−Teller) and Langmuir equations. The Langmuir equation could be used for surfaces covered with a single layer of gas; the BET equation, on the other hand, could be applied to multilayer models.

Preparation of Nanocomposite Thin Films and Coating on UV-LED Devices. Various amounts of polyvinyl alcohol (average M_w = 13k, 567 mg for 10 wt %, 252 mg for 20 wt %, 147 mg for 30 wt %, 94.5 mg for 40 wt %, and 63 mg for 50 wt %) were dissolved in 3 mL of **NP1** water solution (21 mg/mL) and the mixtures were sonicated for 1 h. They were then fabricated on quartz substrates by spin-casting at 2000 rpm for 30 s. Ultraviolet LEDs were purchased from Seoul Optodevice Co., Ltd. (Part No. P8D236), and the polymer thin film was coated on the lens (silicone resin) of LEDs by solvent casting.

REFERENCES AND NOTES

1. Colombo, M. G.; Hauser, A.; Guedel, H. U. Evidence for strong mixing between the LC and MLCT excited states in bis(2-phenylpyridinato-C2, N′)(2,2′-bipyridine)iridium(III). *Inorg. Chem.* **1993**, *32*, 3088–3092.
2. Adachi, C.; Kwong, R. C.; Djurovich, P.; Adamovich, V.; Baldo, M. A.; Thompson, M. E.; Forrest, S. R. Endothermic energy transfer: A mechanism for generating very efficient high-energy phosphorescent emission in organic materials. *Appl. Phys. Lett.* **2001**, *79*, 2082–2084.
3. Lamansky, S.; Djurovich, P.; Murphy, D.; Abdel-Razzaq, F.; Kwong, R.; Tsyba, I.; Bortz, M.; Mui, B.; Bau, R.; Thompson, M. E. Synthesis and characterization of phosphorescent cyclometalated iridium complexes. *Inorg. Chem.* **2001**, *40*, 1704–1711.
4. Tamayo, A. B.; Alleyne, B. D.; Djurovich, P. I.; Lamansky, S.; Tsyba, I.; Ho, N. N.; Bau, R.; Thompson, M. E. Synthesis and characterization of facial and meridional tris-cyclometalated iridium(III) complexes. *J. Am. Chem. Soc.* **2003**, *125*, 7377–7378.
5. Holder, E.; Langeveld, B. M. W.; Schubert, U. S. New trends in the use of transition metal-ligand complexes for applications in electroluminescent devices. *Adv. Mater.* **2005**, *17*, 1109–1121.
6. Lowry, M. S.; Bernhard, S. Synthetically tailored excited states: phosphorescent, cyclometalated iridium(III) complexes and their applications. *Chem.—Eur. J.* **2006**, *12*, 7970–7977.
7. So, F.; Kido, J.; Burrows, P. Organic light-emitting devices for solid-state lighting. *MRS Bull.* **2008**, *33*, 663–669.
8. Liu, Q.-D.; Lu, J.; Ding, J.; Tao, Y. Design and synthesis of phosphorescent iridium containing dendrimers for potential applications in organic light-emitting diodes. *Macromol. Chem. Phys.* **2008**, *209*, 1931–1941.
9. Chiu, Y.-C.; Hung, J.-Y.; Chi, Y.; Chen, C.-C.; Chang, C.-H.; Wu, C.-C.; Cheng, Y.-M.; Yu, Y.-C.; Lee, G.-H.; Chou, P.-T. En route to high external quantum efficiency (~12%), organic true-blue-light-emitting diodes employing novel design of iridium (III) phosphors. *Adv. Mater.* **2009**, *21*, 2221–2225.
10. Ma, B.; Kim, B. J.; Poulsen, D. A.; Pastine, S. J.; Fréchet, J. M. J. Multifunctional crosslinkable iridium complexes as hole transporting/electron blocking and emitting materials for solution-processed multilayer organic light-emitting diodes. *Adv. Funct. Mater.* **2009**, *19*, 1024–1031.
11. Pei, Q.; Yu, G.; Zhang, C.; Yang, Y.; Heeger, A. J. Polymer light-emitting electrochemical cells. *Science* **1995**, *269*, 1086–1088.
12. Bolink, H. J.; Coronado, E.; Costa, R. D.; Ortí, E.; Sessolo, M.; Graber, S.; Doyle, K.; Neuburger, M.; Housecroft, C. E.; Constable, E. C. Long-living light-emitting electrochemical cells—control through supramolecular interactions. *Adv. Mater.* **2008**, *20*, 3910–3913.
13. Kim, J. I.; Shin, I.-S.; Kim, H.; Lee, J.-K. Efficient electrogenerated chemiluminescence from cyclometalated iridium(III) complexes. *J. Am. Chem. Soc.* **2005**, *127*, 1614–1615.
14. Shin, I.-S.; Kim, J. I.; Kwon, T.-H.; Hong, J.-I.; Lee, J.-K.; Kim, H. Efficient electrogenerated chemiluminescence from bis-cyclometalated iridium(iii) complexes with substituted 2-phenylquinoline ligands. *J. Phys. Chem. C* **2007**, *111*, 2280–2286.
15. Zanarini, S.; Rampazzo, E.; Bonacchi, S.; Juris, R.; Marcaccio, M.; Montalti, M.; Paolucci, F.; Prodi, L. Iridium doped silica-PEG nanoparticles: enabling electrochemiluminescence of neutral complexes in aqueous media. *J. Am. Chem. Soc.* **2009**, *131*, 14208–14209.
16. Yu, M.; Zhao, Q.; Shi, L.; Li, F.; Zhou, Z.; Yang, H.; Yi, T.; Huang, C. Cationic iridium(III) complexes for phosphorescence staining in the cytoplasm of living cells. *Chem. Commun.* **2008**, 2115–2117.
17. Lo, K. K.-W.; Hui, W.-K.; Chung, C.-K.; Tsang, K. H.-K.; Ng, D. C.-M.; Zhu, N.; Cheung, K.-K. Biological labelling reagents and probes derived from luminescent transition metal polypyridine complexes. *Coord. Chem. Rev.* **2005**, *249*, 1434–1450.
18. Ma, D.-L.; Wong, W.-L.; Chung, W.-H.; Chan, F.-Y.; So, P.-K.; Lai, T.-S.; Zhou, Z.-Y.; Leung, Y.-C.; Wong, K.-Y. A highly selective luminescent switch-on probe for histidine/histidine-rich proteins and its application in protein staining. *Angew. Chem., Int. Ed.* **2008**, *47*, 3735–3739.
19. Chen, H.; Zhao, Q.; Wu, Y.; Li, F.; Yang, H.; Yi, T.; Huang, C. Selective phosphorescence chemosensor for homocysteine based on an iridium(III) complex. *Inorg. Chem.* **2007**, *46*, 11075–11081.
20. Lai, C.-W.; Wang, Y.-H.; Lai, C.-H.; Yang, M.-J.; Chen, C.-Y.; Chou, P.-T.; Chan, C.-S.; Chi, Y.; Chen, Y.-C.; Hsiao, J.-K.

Iridium-complex-functionalized Fe$_3$O$_4$/SiO$_2$ core/shell nanoparticles: a facile three-in-one system in magnetic resonance imaging, luminescence imaging, and photodynamic therapy. *Small* **2008**, *4*, 218–224.

21. Lo, K. K.-W.; Ng, D. C.-M.; Chung, C.-K. First examples of luminescent cyclometalated iridium(III) complexes as labeling reagents for biological substrates. *Organometallics* **2001**, *20*, 4999–5001.

22. Burns, A.; Ow, H.; Wiesner, U. Fluorescent core-shell silica nanoparticles: towards "lab on a particle" architectures for nanobiotechnology. *Chem. Soc. Rev.* **2006**, *35*, 1028–1042.

23. Wang, F.; Tan, W. B.; Zhang, Y.; Fan, X.; Wang, M. Luminescent nanomaterials for biological labelling. *Nanotechnology* **2006**, *17*, R1–R13.

24. Rampazzo, E.; Bonacchi, S.; Montalti, M.; Prodi, L.; Zaccheroni, N. Self-organizing core-shell nanostructures: spontaneous accumulation of dye in the core of doped silica nanoparticles. *J. Am. Chem. Soc.* **2007**, *129*, 14251–14256.

25. Ow, H.; Larson, D. R.; Srivastava, M.; Baird, B. A.; Webb, W. W.; Wiesner, U. Bright and stable core-shell fluorescent silica nanoparticles. *Nano Lett.* **2005**, *5*, 113–117.

26. Rossi, L. M.; Shi, L.; Quina, F. H.; Rosenzweig, Z. Stöber synthesis of monodispersed luminescent silica nanoparticles for bioanalytical assays. *Langmuir* **2005**, *21*, 4277–4280.

27. Blaaderen, A. v.; Vrij, A. Synthesis and characterization of monodisperse colloidal organo-silica spheres. *J. Colloid Interface Sci.* **1993**, *156*, 1–18.

28. Ha, S.-W.; Camalier, C. E.; Beck, G. R., Jr.; Lee, J.-K. New method to prepare very stable and biocompatible fluorescent silica nanoparticles. *Chem. Commun.* **2009**, 2881–2883.

29. Stöber, W.; Fink, A.; Bohn, E. Controlled growth of monodisperse silica spheres in the micron size range. *J. Colloid Interface Sci.* **1968**, *26*, 62–69.

30. Nakamaru, K. Synthesis, luminescence quantum yield and lifetime of trischelated ruthenium(II) mixed-ligand complexes including 3,3′-dimethyl-2,2′-bipyridyl. *Bull. Chem. Soc. Jpn.* **1982**, *55*, 2697–2705.

31. Vacha, M.; Koide, Y.; Kotani, M.; Sato, H. Photobleaching and single molecule detection of a phosphorescent organometallic iridium(III) complex. *J. Lumin.* **2004**, *107*, 51–56.

32. Santra, S.; Zhang, P.; Wang, K.; Tapec, R.; Tan, W. Conjugation of biomolecules with luminophore-doped silica nanoparticles for photostable biomarkers. *Anal. Chem.* **2001**, *73*, 4988–4993.

33. Sing, K. S. W.; Everett, D. H.; Haul, R. A. W.; Moscou, L.; Pierotti, R. A.; Rouquerol, J.; Siemieniewska, T. Reporting physisorption data for gas/solid systems with special reference to the determination of surface area and porosity. *Pure Appl. Chem.* **1985**, *57*, 603–619.

34. Pimputkar, S.; Speck, J. S.; DenBaars, S. P.; Nakamura, S. Prospects for LED lighting. *Nat. Photonics* **2009**, *3*, 180–182.

35. Nonoyama, M. Benzo[h]quinolin-10-yl-N Iridium(III) Complexes. *Bull. Chem. Soc. Jpn.* **1974**, *47*, 767–768.

36. Sabourault, N.; Mignani, G.; Wagner, A.; Mioskowski, C. Platinum oxide (PtO$_2$): a potent hydrosilylation catalyst. *Org. Lett.* **2002**, *4*, 2117–2119.